

# Solution-State NMR Studies of the Surface Structure and Dynamics of Semiconductor Nanocrystals

**Joseph R. Sachleben\***

*Campus Chemical Instrument Center, The Ohio State University, Johnston Laboratory 119,  
176 West 18th Avenue, Columbus, Ohio 43210*

**Vicki Colvin**

*Department of Chemistry, Rice University, Houston, Texas 77005*

**Lyndon Emsley**

*Laboratoire de Stéréochimie et des Interactions Moléculaires, UMR-117 (CNRS/ENS-Lyon),  
Ecole Normale Supérieure de Lyon, 69364 Lyon, France*

**E. Wrenn Wooten and A. Paul Alivisatos**

*Materials Sciences Division, Lawrence Berkeley Laboratory, and Department of Chemistry,  
University of California, Berkeley, California 94720*

*Received: April 27, 1998; In Final Form: July 31, 1998*

$^1\text{H}$  and  $^{13}\text{C}$  nuclear magnetic resonance (NMR) relaxation studies of thiophenol-capped CdS nanocrystals are presented. The transverse and longitudinal relaxation times were investigated as a function of nanocrystal radius, and the transverse relaxation time was also studied as a function of temperature. Both proton and carbon  $T_2$  values were found to increase with nanocrystal radius, contrary to initial expectations. This effect is explained in terms of motion of the thiophenol with respect to the nanocrystalline surface. Theoretical expressions for relaxation due to anisotropic motion are developed based on both bridging and terminal bonding configurations of the thiophenol ligands, and the data are fit to these models. The data are found to be consistent with thiophenol ligands bound in a terminal fashion to a single Cd atom. The temperature dependence of the proton  $T_2$  value is also surprising.  $T_2$  is found to decrease with increasing temperature, and the size of this change scales with the nanocrystal radius. This is explained in terms of an extra component of relaxation due to thermally excited electrons.

## Introduction

Semiconductor nanocrystals are small particles that are intermediate between molecular and bulk phases, which leads to their physical properties being size dependent.<sup>1,2</sup> For example, the frequency at which light is absorbed (and thus the color of the sample) depends on the radius of the nanocrystal. These size-dependent properties have potential to be tuned for technological purposes.<sup>3–5</sup> However, before nanocrystals can be used in devices, the relationship between the structure of the nanocrystal and its properties needs to be understood.

The structure of a nanocrystal can be loosely divided into two parts: the surface, which is usually covered with organic capping groups, and the core (or interior). This study addresses the surface, which, not surprisingly, plays an important role in determining many nanocrystalline properties. For example, trapping of the optically produced hole, the fluorescence of the nanocrystal, and the surface energy (and hence the phase diagram) all depend on the structure of the surface.<sup>6</sup> Not only does the surface affect the physical properties of the nanocrystal, but it is often necessary to synthetically manipulate the nanocrystal surface so as to achieve solubility in organic solvents. Therefore, a study of the organic molecules bound to the surface of the nanocrystal is crucial to a detailed understanding of these systems, and despite its importance, the

surface structure of these particles has so far received relatively little attention.<sup>7–10</sup>

Both the rearrangement of the surface atoms from their positions in the bulk semiconductor and the bonding configuration and distribution of surface ligands affect the properties of the nanocrystal. In this paper, we utilize proton and carbon nuclear magnetic resonance (NMR) spectroscopy to investigate the surface structure and dynamics of thiophenol-capped CdS nanocrystals. In the past,<sup>9</sup> such studies have determined the surface coverage of the nanocrystal and the number of different ligand environments on the surface. However, this study did not provide an assignment of the chemical shift to the bonding geometry of the thiophenol on the nanocrystal surface. We have extended our studies of the surface by measuring  $^1\text{H}$  and  $^{13}\text{C}$  NMR relaxation in order to investigate the bonding configuration and dynamics of the thiophenol ligands.

The thiophenol ligands on the nanocrystal surface provide a model system for NMR relaxation studies. The ligands are isolated from one another so that relaxation is primarily due to dipolar couplings within each ligand. The possible motions are simple once the bonding arrangement of the ligand is determined and are conveniently described using Woessner models.<sup>11,12</sup> In this article, we present an examination of the dependencies on size and temperature of the  $^1\text{H}$  and  $^{13}\text{C}$  transverse and

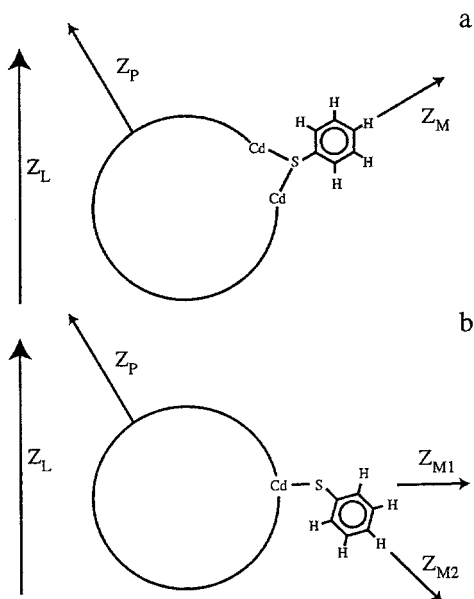


**Figure 1.** Axis systems used to define the orientation of the thiophenol ligand. The principal axis system of the dipolar interaction (PAS) is not shown explicitly. It is defined by the internuclear vector relevant to the relaxation process being investigated: (a) ligand in a bridging configuration, (b) terminal configuration.

longitudinal relaxation times of the ligands on thiophenol-capped CdS nanocrystals. The data are interpreted in terms of dipolar relaxation governed by motional models based on both bridging and terminally bound thiophenol ligands. Correlation times for the appropriate motions are estimated. We find that the data are more consistent with terminally bound thiophenol ligands, however, the data are not perfectly described by either model. Additional relaxation mechanisms, such as that due to chemical-shift anisotropy and librational motions, cause these discrepancies. In support of this hypothesis, we show that the temperature dependence of the relaxation behavior cannot be completely explained by the most simple motional models and a novel paramagnetic relaxation mechanism due to thermally excited electrons is postulated to explain the unusual temperature behavior.

## Theoretical

Model compounds containing Cd, S, and thiophenol have been synthesized and characterized by X-ray crystallography,<sup>13–15</sup> and these compounds show that thiophenol molecules can bind either in a bridging manner to two cadmium atoms or terminally to a single cadmium atom. The crystal structure of a single-sized small CdS nanocrystal has been obtained<sup>16</sup> and shows that the thiophenols in this sample are bound in a bridging fashion. These crystallographic results suggest that relevant motional models for the thiophenol ligands on the nanocrystal surface should be based on either bridging or terminal thiophenol molecules. A schematic drawing of these bonding arrangements is shown in Figure 1 along with the definition of the various axis systems used. The principal axis system of the dipole–dipole interaction is not explicitly indicated in Figure 1 because it depends on which nucleus is examined. Because the motion of the ligand is different in the two arrangements, relaxation studies should allow us to distinguish between the two types of bonding. We have developed theoretical models for both situations, which are described below.

To understand the relaxation data presented in this paper, detailed relaxation calculations must be presented. The equa-

**TABLE 1: Longitudinal and Transverse Relaxation Rates for <sup>1</sup>H and <sup>13</sup>C Dipolar Relaxation<sup>20</sup>**

<sup>1</sup> H dipole–dipole relaxation	$T_1^{-1} = 3J(\omega_0) + 12J(2\omega_0)$
	$T_2^{-1} = 1/2[9J(0) + 15J(\omega_0) + 6J(2\omega_0)]$
<sup>13</sup> C dipole–dipole relaxation	$T_1^{-1} = J(\omega_C - \omega_H) + 3J(\omega_C) +$
	$6J(\omega_C + \omega_H)$
	$T_2^{-1} = 1/2[4J(0) + J(\omega_C - \omega_H)$
	$3J(\omega_C) + 6J(\omega_H) + 6J(\omega_C + \omega_H)]$

tions for calculating  $T_1$  and  $T_2$  are derived from Redfield theory,<sup>17–19</sup> assuming only two spin interactions without  $J$  couplings. These equations are the same as those presented by Szabo<sup>20</sup> with only a slight change of the definition of the spectral density. These equations only approximately describe our system and entirely neglect cross-correlation effects. We will show that this is a good approximation because the nanocrystals are tumbling in the slow-motion regime in which cross-correlation effects are in any case negligible.

Table 1 gives the expressions for transverse and longitudinal relaxation rates as a function of the spectral densities for homonuclear and heteronuclear spin pairs. The spectral densities are calculated by taking the real Fourier transforms of the correlation function of the dipolar coupling<sup>20,21</sup>

$$J_q(\omega) = 2 \int_0^\infty C_q(t) \cos(\omega t) dt \quad (1)$$

where the dipolar correlation function is given by

$$C_q(t) = \frac{\pi}{5} \left( \frac{\mu_0}{4\pi} \right)^2 \hbar^2 \gamma_I^2 \gamma_S^2 \left\langle \frac{Y_{2,q}(\theta_{LF}^{ij}(0), \phi_{LF}^{ij}(0)) Y_{2,q}^*(\theta_{LF}^{ij}(t), \phi_{LF}^{ij}(t))}{r(0)^3 r(t)^3} \right\rangle \quad (2)$$

The correlation function is written in terms of the spherical harmonics,  $Y_{2,q}(\theta_{LF}^{ij}(t), \phi_{LF}^{ij}(t))$ , with  $\theta_{LF}^{ij}(t)$  and  $\phi_{LF}^{ij}(t)$  being the polar and azimuthal angles, respectively, of the internuclear vector of spin pair  $ij$  in the laboratory frame at time  $t$  and  $\gamma_I$  and  $\gamma_S$  are the gyromagnetic ratios. Throughout this paper,  $I$  and  $S$  will either be two <sup>1</sup>H nuclei or a <sup>1</sup>H and a <sup>13</sup>C, depending on whether proton or carbon relaxation is being considered. When the gyromagnetic ratios are in units of  $\text{rad s}^{-1} \text{T}^{-1}$  and  $\hbar$  in  $\text{J s rad}^{-1}$ , the units of  $C_q(t)$  are  $\text{Hz}^2$ .

In the following discussion, we use two models of the motion of the thiophenol ligands, corresponding to bridging and terminal, to derive correlation functions and spectral densities. These expressions apply to both the carbon and proton cases, except that in the proton case, we assume the effects of multiple spins are additive and in the carbon case, that only the bound proton is responsible for the relaxation of the carbon. We neglect other sources of relaxation such as that due to the chemical-shift anisotropy. These calculations are used to model the relaxation data presented later in this paper.

Of the two configurations, bridging thiophenol molecules are the easier to consider because fewer rotations are needed to express the dipole–dipole interaction in the relevant nanocrystal-defined frames illustrated in Figure 1a. Making the appropriate rotations to these frames using the Wigner rotation matrices,  $D_{lm}^{(2)}(\Omega)$ ,<sup>21–23</sup>  $Y_{2,q}(\theta_{LF}^{ij}(t), \phi_{LF}^{ij}(t))$  becomes

$$Y_{2,q}(\theta_{LF}^{ij}(t), \phi_{LF}^{ij}(t)) = \sum_{m,n} D_{q,m}^{(2)}(\Omega_{L \rightarrow P}, t) D_{m,n}^{(2)}(\Omega_{P \rightarrow M}, t) Y_{2,n}(\theta_{M \rightarrow PAS}^{ij}, \phi_{M \rightarrow PAS}^{ij}) \quad (3)$$

where  $\Omega_{L \rightarrow P}$  are the Euler angles between the lab frame and the axis system fixed on the nanocrystal,  $\Omega_{P \rightarrow M}$  are the angles between the particle-fixed axis system and the thiophenol-fixed axis system, and  $\theta_{M \rightarrow PAS}^{ij}$  and  $\theta_{M \rightarrow PAS}$  are the angles between the thiophenol-fixed axis system and the principal axis system of the dipolar interaction. These different axis systems are illustrated in Figure 1. The thiophenol-fixed axis system denoted by  $M$ , has its  $z$  axis along the S-C bond and the  $x$  axis in the plane of the thiophenol ring. The spherical harmonic specifying the direction of the internuclear vector is time independent in this frame and is fully specified by the angle  $\theta_{M \rightarrow PAS}^{ij}$ . The angle  $\phi_{M \rightarrow PAS}^{ij}$  is zero. The correlation function then becomes

$$C_q(t) = \frac{\pi}{5} \omega_D^2 \sum_{\substack{m,n \\ m',n'}} \langle D_{q,m}^{(2)}(\Omega_{L \rightarrow P}) D_{q,m'}^{(2)}(\Omega'_{L \rightarrow P})^* \rangle \times \\ \langle D_{m,n}^{(2)}(\Omega_{P \rightarrow M}) D_{m',n'}^{(2)}(\Omega'_{P \rightarrow M})^* \rangle \times \\ Y_{2,n}(\theta_{M \rightarrow PAS}^{ij}, 0) Y_{2,n'}^*(\theta_{M \rightarrow PAS}^{ij}, 0) \quad (4)$$

where

$$\omega_D = \left( \frac{\mu_0}{4\pi} \right) \frac{\gamma \gamma' S}{r^3}$$

and where the unprimed euler angles,  $\Omega$ , correspond to the angles at time 0, the primed angles are the angles at time  $t$ , and the angular brackets indicate an ensemble average over all initial and final orientations of the internuclear vector. In eq 4, we have assumed that the overall tumbling of the nanocrystal is uncorrelated with the internal rotations of the thiophenol molecules, thereby allowing the separation of the ensemble average for the overall tumbling of the whole particle and the internal motions of the ligands. This assumption implies that the “internal” correlation time of the ligand motion must be much shorter than the “overall” correlation time of the whole particle. If the overall tumbling of the nanocrystal is isotropic, the ensemble average has been shown to be<sup>20</sup>

$$\langle D_{q,m}^{(2)}(\Omega_{L \rightarrow P}) D_{q,m'}^{(2)}(\Omega'_{L \rightarrow P})^* \rangle = \frac{1}{5} \delta_{m,m'} e^{-t/t_m} \quad (5)$$

where  $t_m$  is the correlation time characteristic of isotropic rotational diffusion of the nanocrystal. For isotropic motion, the  $q$  index is unimportant and it will be dropped in the following. Using eq 5, the definition of the Wigner rotation matrix element

$$D_{m,n}^{(j)}(\alpha, \beta, \gamma) = e^{-im\alpha} d_{m,n}^{(j)}(\beta) e^{-iny} \quad (6)$$

and the orthogonality relation of the reduced matrix elements,  $d_{m,n}^{(j)}(\beta)$ ,<sup>21-23</sup>

$$\sum_m d_{m,n}^{(j)}(\beta) d_{m,n'}^{(j)}(\beta) = \delta_{n,n'} \quad (7)$$

the correlation function in eq 4 simplifies to

$$C(t) = \frac{\pi}{25} \omega_D^2 e^{-t/t_m} \sum_n |Y_{2,n}(\theta_{M \rightarrow PAS}^{ij}, 0)|^2 \langle e^{in(\gamma'_{P \rightarrow M} - \gamma_{P \rightarrow M})} \rangle \quad (8)$$

Only the real part of the correlation function contributes to the spectral density, and thus, eq 8 becomes

$$C(t) = \frac{\pi}{25} \omega_D^2 e^{-t/t_m} \sum_n |Y_{2,n}(\theta_{M \rightarrow PAS}^{ij}, 0)|^2 \times \\ \langle \cos[n(\gamma'_{P \rightarrow M} - \gamma_{P \rightarrow M})] \rangle \quad (9)$$

To evaluate this correlation function, we integrate over all initial and final configurations of the thiophenol

$$\langle \cos[n(\gamma'_{P \rightarrow M} - \gamma_{P \rightarrow M})] \rangle = \\ P_{\text{eq}} \int_0^{2\pi} \int_0^{2\pi} p(\gamma'_{P \rightarrow M}, t | \gamma_{P \rightarrow M}, 0) \times \\ \cos[n(\gamma'_{P \rightarrow M} - \gamma_{P \rightarrow M})] d\gamma'_{P \rightarrow M} d\gamma_{P \rightarrow M} \quad (10)$$

where  $P_{\text{eq}}$  is the equilibrium probability of finding the thiophenol ligand orientated at some angle  $\gamma_{P \rightarrow M}$  and  $p(\gamma'_{P \rightarrow M}, t | \gamma_{P \rightarrow M}, 0)$  is the conditional probability that a molecule at angle  $\gamma_{P \rightarrow M}$  at time 0 will be at  $\gamma'_{P \rightarrow M}$  at time  $t$ . In this theory, different models of the motion are distinguished by these conditional probabilities.

Using the conditional probability for rotational diffusion of the thiophenol ligand, derived in the Appendix 1

$$p(\gamma', t | \gamma, 0) = \frac{1}{2\pi} + \frac{1}{\pi} e^{-t/t_i} \cos(\gamma' - \gamma) \quad (11)$$

where  $t_i$  is the correlation time for the motion of the thiophenol with respect to the nanocrystal surface, we calculate the ensemble average of eq 10

$$\langle \cos[n(\gamma'_{P \rightarrow M} - \gamma_{P \rightarrow M})] \rangle = P_{\text{eq}} \int_0^{2\pi} \int_0^{2\pi} \left[ \frac{1}{2\pi} + \frac{1}{\pi} e^{-t/t_i} \cos(\gamma' - \gamma) \right] \cos[n(\gamma'_{P \rightarrow M} - \gamma_{P \rightarrow M})] d\gamma'_{P \rightarrow M} d\gamma_{P \rightarrow M} = \\ \begin{cases} 1 & \text{for } n = 0 \\ e^{-t/t_i} & \text{for } n = \pm 1 \\ 0 & \text{for } n = \pm 2 \end{cases} \quad (12)$$

where we have used  $P_{\text{eq}} = 1/2\pi$ . Combining eqs 9 and 12, the correlation function for a bridging thiophenol ligand undergoing rotational diffusion is found to be

$$C(t) = \frac{\pi}{25} \omega_D^2 \{ |Y_{2,0}(\theta_{M \rightarrow PAS}^{ij}, 0)|^2 e^{-t/t_m} + \\ 2 |Y_{2,1}(\theta_{M \rightarrow PAS}^{ij}, 0)|^2 e^{-(1/t_m + 1/t_i)t} \} \quad (13)$$

Finally, Fourier transformation of this correlation function gives the corresponding spectral density

$$J(\omega) = \frac{2\pi}{25} \omega_D^2 \left\{ \left| Y_{2,0}(\theta_{M \rightarrow PAS}^{ij}, 0) \right|^2 \frac{1/t_m}{(1/t_m)^2 + \omega^2} + \right. \\ \left. 2 \left| Y_{2,1}(\theta_{M \rightarrow PAS}^{ij}, 0) \right|^2 \frac{1/t_m + 1/t_i}{(1/t_m + 1/t_i)^2 + \omega^2} \right\} \quad (14)$$

which can be used to calculate the relaxation times.

The relaxation expressions for terminal thiophenol ligands can be calculated similarly. In Appendix 2, we calculate the correlation function for the terminal ligands. This correlation function is shown in eq A2-6 (Appendix 2). The spectral density is found after Fourier transforming this correlation function to be

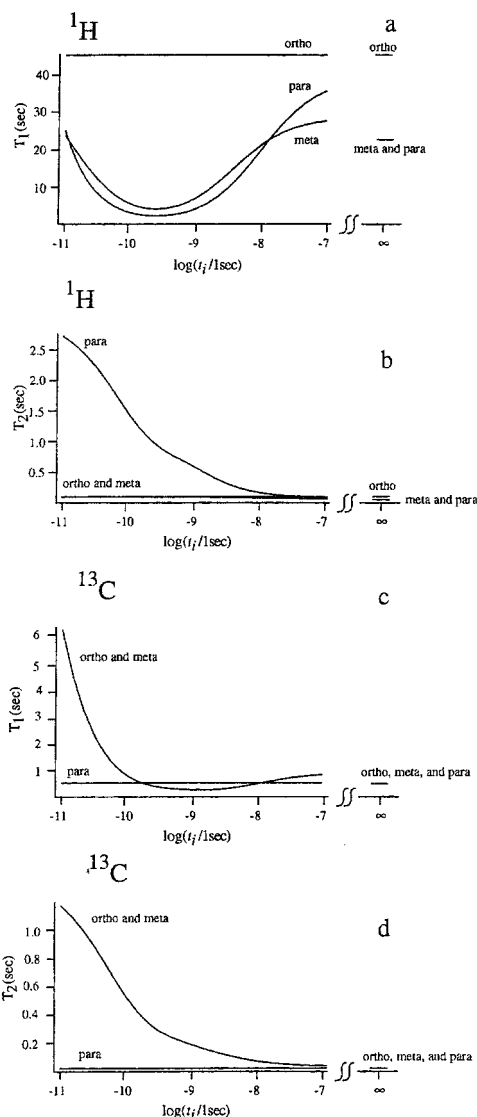


**Figure 2.** Simulations of proton and carbon  $T_1$  and  $T_2$  as a function of the C-S rotational correlation time,  $t_i$ , assuming that the thiophenol is bridgingly bound and undergoing rotational diffusion about this bond. The overall rotational correlation time is set to 10 ns. (a) Proton  $T_1$  versus  $\log(t_i)$ . (b) Proton  $T_2$  versus  $\log(t_i)$ . (c) Carbon  $T_1$  versus  $\log(t_i)$ . (d) Carbon  $T_2$  versus  $\log(t_i)$ . The infinity values correspond to the values calculated with a pure isotropic tumbling model using a correlation time of 10 ns.

$$\begin{aligned}
 J(\omega) = & \frac{2\pi}{25} \omega_D^2 \left\{ \left| d_{0,0}^{(2)}(\beta_{M1-M2}) \right|^2 \left| Y_{2,0}(\theta_{M2 \rightarrow PAS}^{ij}, 0) \right|^2 \frac{1/t_m}{(1/t_m)^2 + \omega^2} + \right. \\
 & 2 \left| d_{1,0}^{(2)}(\beta_{M1-M2}) \right|^2 \left| Y_{2,0}(\theta_{M2 \rightarrow PAS}^{ij}, 0) \right|^2 \frac{1/t_m + 1/t_{i1}}{(1/t_m + 1/t_{i1})^2 + \omega^2} + \\
 & 2 \left| d_{1,0}^{(2)}(\beta_{M1-M2}) \right|^2 \left| Y_{2,1}(\theta_{M2 \rightarrow PAS}^{ij}, 0) \right|^2 \frac{1/t_m + 1/t_{i2}}{(1/t_m + 1/t_{i2})^2 + \omega^2} + \\
 & 2(|d_{1,1}^{(2)}(\beta_{M1-M2})|^2 + |d_{1,-1}^{(2)}(\beta_{M1-M2})|^2) \times \\
 & \left. \left| Y_{2,1}(\theta_{M2 \rightarrow PAS}^{ij}, 0) \right|^2 \frac{1/t_m + 1/t_{i1} + 1/t_{i2}}{(1/t_m + 1/t_{i1} + 1/t_{i2})^2 + \omega^2} \right\} \quad (15)
 \end{aligned}$$

Equations 14 and 15 are the spectral densities for bridging and terminally bonded thiophenol ligands, respectively, and are the basic functions necessary for calculating relaxation rates. These spectral densities consist of a sum of Lorentzian lines,

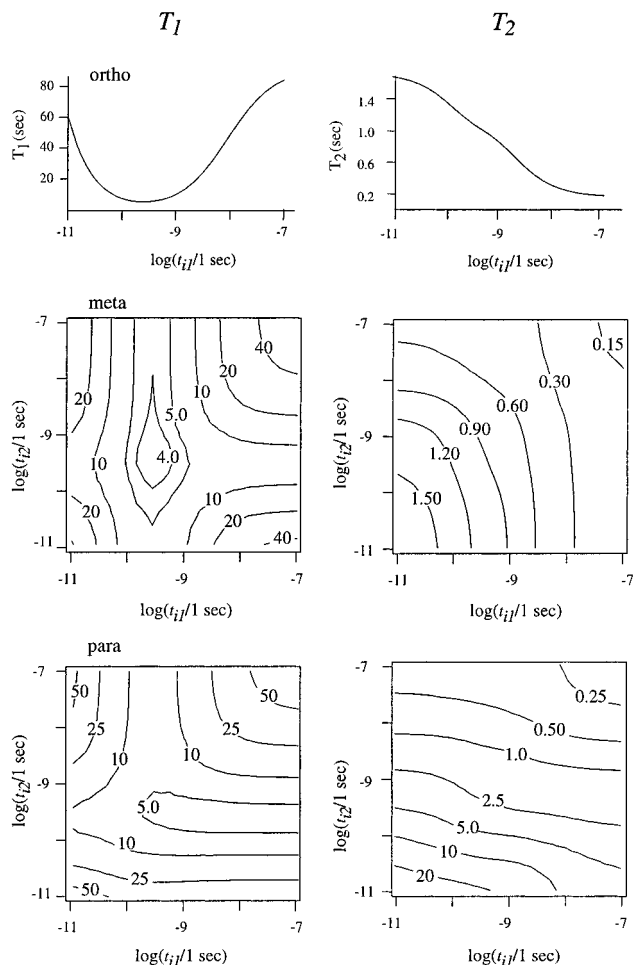


**Figure 3.** Simulations of the proton  $T_1$  and  $T_2$  as a function of the logarithm of the Cd-S and S-C rotational correlation times,  $\log(t_{i1})$  and  $\log(t_{i2})$ , assuming that the thiophenol is terminally bound and undergoing rotational diffusion about both bonds. The overall correlation time,  $t_m$ , was set at 10 ns.

centered at zero frequency, with widths given by linear combinations of the inverse correlation times and whose intensities are proportional to the spherical harmonics that relate the molecular axis system to the principal axis system of the dipolar pair being considered. These spherical harmonic functions are determined completely by the molecular geometry and, thus, differentiate the relaxation for the various sites in the thiophenol ligand. Figures 2-4 show the results of the theoretical calculations of  $^1\text{H}$  and  $^{13}\text{C}$  relaxation times for the two motional models.

For bridging thiophenol ligands (Figure 2), our theoretical results indicate several expected trends. First, the ortho proton and the para carbon relaxation rates are independent of the internal motion. In these two cases, the internuclear vector between the observed nucleus and that responsible for its relaxation is collinear with the S-C bond. In this case, the internal motion does not cause the internuclear vector to fluctuate and the spectral density in eq 14 reduces to

$$J(\omega) = \frac{1}{10} \omega_D^2 \frac{1/t_m}{(1/t_m)^2 + \omega^2} \quad (16)$$

which is the spectral density for a randomly tumbling sphere. Second, it is expected that in the limit of long internal correlation times with respect to that for overall tumbling, all the relaxation times should be given by the isotropically tumbling sphere

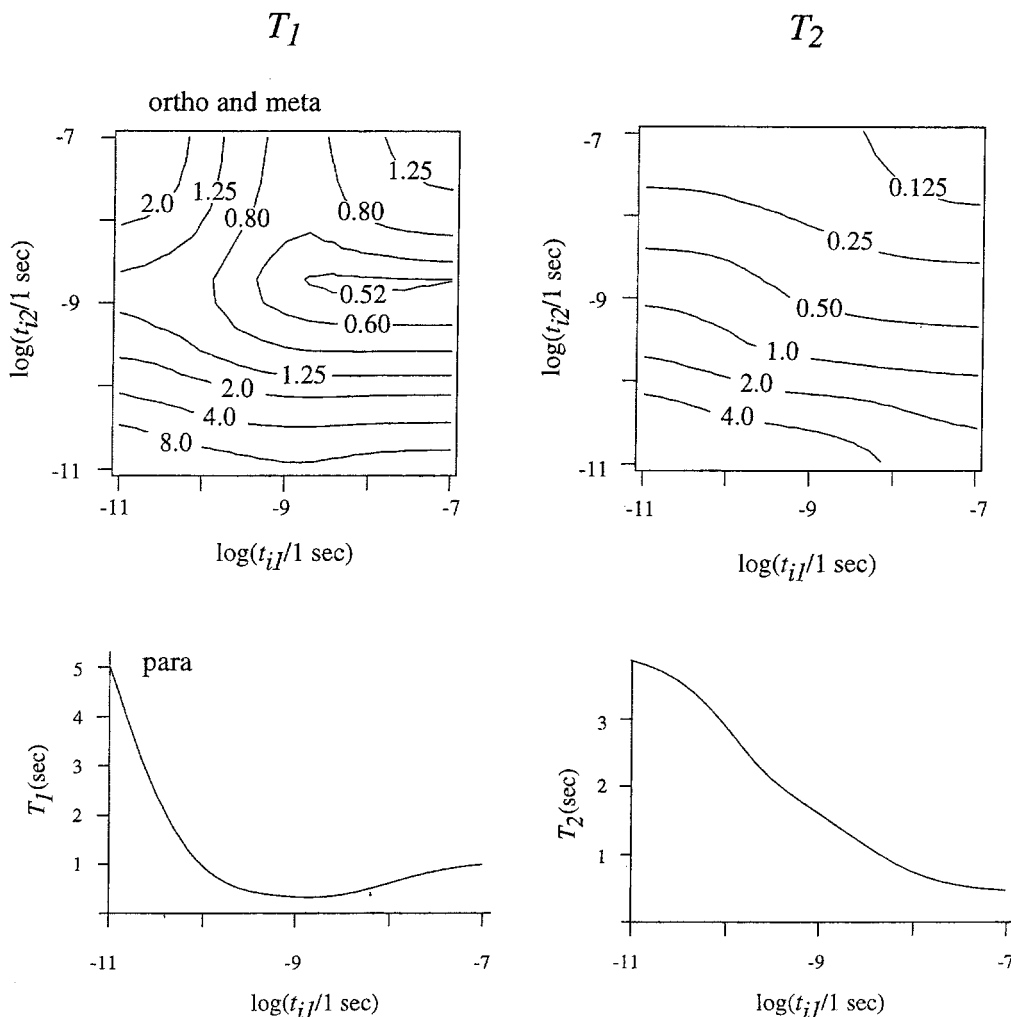


**Figure 4.** Simulations of the  $^{13}\text{C}$   $T_1$  and  $T_2$  as a function of the logarithm of the Cd-S and S-C rotational correlation times,  $\log(t_{i1})$  and  $\log(t_{i2})$ , assuming that the thiophenol is terminally bound and undergoing rotational diffusion about both bonds. The overall correlation time,  $t_m$ , was set at 10 ns.

model, eq 16. These relaxation rates are plotted in Figure 2 as the infinite internal correlation times. However, due to the approximation that the internal and overall motions are not correlated, this does not occur, highlighting that our theoretical results are limited to the case where the internal correlation times are shorter than that for the overall tumbling of the nanocrystal,  $t_i < t_m$ .

Figures 3 and 4 show the theoretical results for terminal thiophenol ligands. Because of the additional rotational degree of freedom, the relaxation of the ortho protons and the para carbon now depend on an internal correlation time, those motions about the Cd-S bond. While the order of magnitude of the relaxation times for the two motional models is the same, the relative ordering of the relaxation times and the ratios of the relaxation times depend on the bonding arrangement. By making careful relaxation measurements, insight into the bonding arrangements of the thiophenol ligands can be acquired.

This type of relaxation model can be applied to any capping group on a semiconductor nanocrystal. The relaxation of a hydrogen or carbon site in any nanocrystal ligand can be calculated by following the same procedure as that presented here. First, one rotates the dipolar correlation function, which is written in the laboratory axis system where the  $z$ -axis is along the external magnetic field, to an axis system on the nanocrystal, where the  $z$ -axis is normal to the nanocrystal surface. This axis system reorients with respect to the laboratory axis system

because of the overall tumbling of the nanocrystal. The correlation function then needs to be rotated to a molecular axis system which is conveniently defined according to the ligand molecule. From this axis system, one rotates down the chain of the ligand molecule, stopping when the correlation function is finally written in terms of the principal axis system of the dipolar coupling. In an aliphatic system, these rotations will be to along the C-C bonds of the hydrocarbon and will parametrize the problem with respect to the rotations about these bonds.<sup>11,12</sup> Once a model for the motion is assumed, the correlation function can be Fourier transformed to give the spectral density for this motion and the relaxation times can be calculated. While this method is computationally heavy, it allows investigation of systems that are unapproachable by other methods.

### Experimental Section

**Synthesis of the Nanocrystals.** Cadmium sulfide nanocrystals were prepared in inverse micelles following standard procedures.<sup>24-26</sup> Two separate solutions of 500.0 mL of spectrographic-grade heptane and 44.4 g of dioctyl sulfosuccinate, AOT, were prepared under nitrogen.  $\text{Cd}(\text{ClO}_4)_2 \cdot 6\text{H}_2\text{O}$  (2.34 g) dissolved in 12.0 mL of deoxygenated deionized water was added to one solution, while 0.36 g of  $\text{Na}_2\text{S} \cdot 9\text{H}_2\text{O}$  dissolved in 12.0 mL of deoxygenated deionized water was added to the other solution. Both solutions appeared clear and

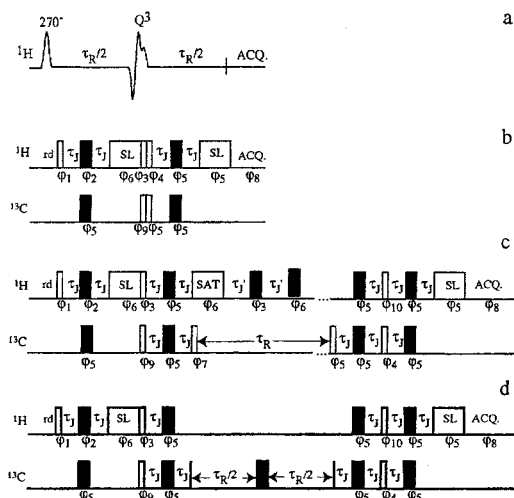


**Figure 5.** Pulse sequences. (a) Sequence for the selective  $T_2$  experiment. See text for details. (b) Double-INEPT experiment used to observe the proton-detected  $^{13}\text{C}$  spectrum shown in Figure 7. Unfilled rectangles represent  $90^\circ$  pulses, filled rectangles represent  $180^\circ$  pulse, and rectangles labeled with SL are spin-lock pulses. (c) Double-INEPT  $T_1$  experiment used to measure  $^{13}\text{C}$  longitudinal relaxation times. The pulse labeled SAT was used to saturate the  $^1\text{H}$  resonances which were kept saturated by repeated  $180^\circ$  pulses. The saturation pulse length was 0.5 ms, and the  $180^\circ$  degree pulses were applied every 0.5 ms. (d) Double-INEPT  $T_2$  experiment used to measure  $^{13}\text{C}$  transverse relaxation times. In the sequences shown, rd is the recycle delay,  $\tau_J$  is set to  $1/(4J_{\text{HC}})$  and allows build up of  $^1\text{H}$ - $^{13}\text{C}$  antiphase coherence, and the two pulses labeled SL are spin-lock pulses to remove residual proton coherence. Typically we used  $\text{rd} = 20$  s,  $\tau_J = 1.5$  ms, with the two spin-lock pulses being 4 and 1 ms, respectively.

colorless after 1 h of mixing. The cadmium solution was then transferred to the sulfide via a 16-gauge double-transfer needle. The transfer process took 15 min and resulted in the formation of a clear yellow solution. The resulting solution was then treated with 0.45 mg of thiophenol, which binds to the surface of the clusters, causing them to precipitate from the micelles. The resulting powder was vacuum filtered 3 times and rinsed with 300 mL of petroleum ether. Rinsing and filtering left a finely divided yellow powder redissolvable in pyridine. Particle composition was determined by elemental analysis, and the nanocrystal radius was determined from UV spectroscopy. Several preparations were carried out to prepare nanocrystal samples with radii ranging from 10.6 to 19.2 Å with a size distribution of 15%.

**NMR Experiments.** NMR samples of the nanocrystals were prepared by dissolving 5 mg of CdS nanocrystals in 0.5 mL of 100% pyridine- $d_5$  (Aldrich). All NMR spectra were recorded in a field corresponding to a  $^1\text{H}$  resonance frequency of 400.13 MHz with Bruker AM-400 and AM-400X spectrometers at a temperature of 303 K unless otherwise specified.

Transverse relaxation times of the  $^1\text{H}$  resonances of the thiophenol ligands on the CdS nanocrystal surface were measured with the selective Hahn echo technique<sup>27</sup> shown in Figure 5a. Typically, the Gaussian  $270^\circ$  pulses<sup>28</sup> were 20 ms long, while the  $Q^3$  pulse<sup>29</sup> length was 45 ms.  $^1\text{H}$  longitudinal relaxation times were measured using the normal inversion-recovery sequence,<sup>30</sup> with nonselective pulses. Typical selective proton  $T_2$  data of the thiophenol ligands on a CdS nanocrystal are shown in Figure 6a.

The  $^{13}\text{C}$  relaxation times were measured from indirectly detected spectra via the thiophenol protons using the double-INEPT experiment<sup>31–36</sup> shown in Figure 5b. The double INEPT inversion-recovery and Hahn echo sequences used to measure

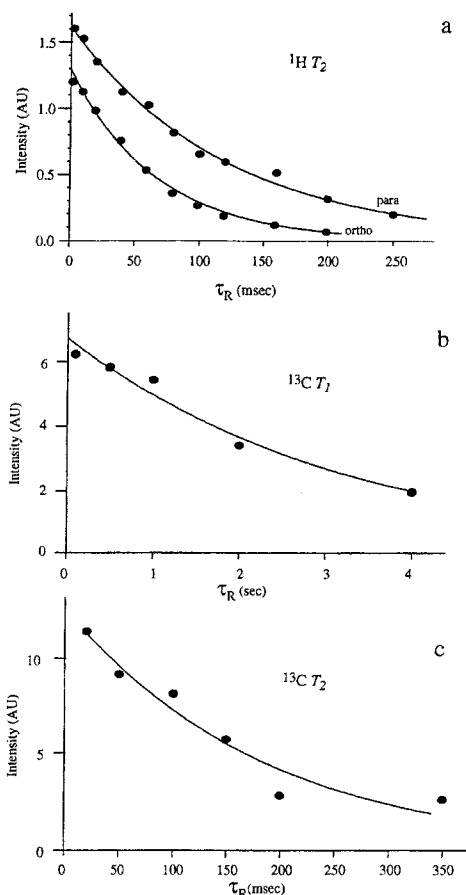


**Figure 6.** Representative relaxation data. (a) Selective  $T_2$  data from the ortho and para protons of the thiophenol ligands on CdS nanocrystals. (b)  $T_1$  data for the para thiophenol carbon on a 15.8 Å radius nanocrystal. (c)  $T_2$  data for the para thiophenol carbon on the same nanocrystal as in b. The experimental time required to record each data set was approximately 12 h. The plotted intensity is the sum of the integrated area of the two members of the doublet seen in the proton-detected carbon spectrum.

the  $^{13}\text{C}$  longitudinal and transverse relaxation times are also shown in Figure 5 (c and d). These sequences are the double-INEPT sequence of Figure 5b, with a  $^{13}\text{C}$  inversion-recovery or Hahn echo sequence inserted. In the case of the inversion-recovery sequence, proton magnetization was saturated while the carbon magnetization recovers so as to ensure that simple monoexponential decays are observed.<sup>37</sup> Figure 6 (b and c) shows typical  $^{13}\text{C}$   $T_1$  and  $T_2$  relaxation data measured on a nanocrystal.

**Computer Modeling and Fitting.** All computer modeling and fitting was done on a Macintosh IIsi computer running either Mathematica 2.0 or specifically written C code. All functions were defined using the results derived above, and these functions were used to generate the plots of the predicted relaxation times shown in Figures 2–4. In all calculations, the phenyl ring of the thiophenol was assumed to be a perfect hexagon with a C–C distance of 1.38 Å, a C–H distance of 1.08 Å, a C–S distance of 1.77 Å,<sup>38</sup> and a Cd–S distance of 2.49 Å.<sup>13</sup> These distances imply that the H–H bond distance in the thiophenol ligands is 2.50 Å and give rise to a static dipolar coupling,  $\omega_D = (\mu_0/4\pi)(\hbar\gamma_1\gamma_2/r^3)$ , between the nearest-neighbor protons of  $\omega_D/2\pi = 7690$  Hz and that between a carbon and its bonded proton of  $\omega_D/2\pi = 24\,000$  Hz. The sulfur of the bridging thiophenol ligands was treated as if it were  $\text{sp}^2$  hybridized, with all bond angles equal to  $120^\circ$ . The hybridization of this sulfur is ultimately unimportant in the calculation because no rotation

about the Cd<sub>2</sub>-S can occur. The Cd-S-C bond angle was assumed to be 115°<sup>13</sup> for the terminal thiophenol ligands. Random fields for <sup>1</sup>H *T*<sub>1</sub> and *T*<sub>2</sub> values and <sup>13</sup>C *T*<sub>1</sub> and *T*<sub>2</sub> values (*R*<sub>1</sub><sup>H</sup>, *R*<sub>2</sub><sup>H</sup>, *R*<sub>1</sub><sup>C</sup>, and *R*<sub>2</sub><sup>C</sup>, respectively) were included to account for relaxation mechanisms other than the dipolar mechanism, such as chemical-shift anisotropy, spin-rotation, and paramagnetic relaxation mechanisms. The random fields were assumed to be independent of the chemical site on the thiophenol ligand, and the total relaxation rate at any site was calculated as the sum of the dipolar rate and the random-field rate. The fits to experimental relaxation times were performed by minimizing the  $\chi^2$  function defined by

$$\chi^2 = \frac{1}{n} \sum_{i=1}^n \frac{(T_i^{\text{exp}} - T_i^{\text{calc}})^2}{\sigma_i^2} \quad (17)$$

where the summation is over all *n* of the data to be fit, *T*<sub>*i*</sub><sup>exp</sup>, is the experimentally determined relaxation time, *T*<sub>*i*</sub><sup>calc</sup> is the relaxation time calculated from the relaxation models, and  $\sigma_i$  is the error in the experimental data. If  $\chi^2$  is less than 1, then all the calculated values are within the error of the experimentally determined values. The fits were done using Powell's quadratically convergent method for multidimensional minimization.<sup>39</sup> To find a global minimum, the fits were repeated 1000 times with random starting positions in the range 10<sup>-5</sup> s >  $\tau_m$  > 10<sup>-10</sup> s, 10<sup>-6</sup> s >  $\tau_i$ ,  $\tau_{i1}$ ,  $\tau_{i2}$  > 10<sup>-13</sup> s, and 10<sup>-2</sup> s<sup>-1</sup> < carbon and proton random fields < 10<sup>2</sup> s<sup>-1</sup> with the best minimum being retained.

## Results and Discussion

**Proton and Carbon Spectra.** A typical <sup>1</sup>H NMR spectrum of thiophenol-capped CdS nanocrystals is shown in Figure 7a. The spectrum has been previously assigned,<sup>9</sup> and the peaks at 8.71, 7.19, and 7.56 ppm are due to the ortho, meta, and para protons, respectively, of residual protonated pyridine co-purified from the synthesis procedure. These resonances are identical to those for pure pyridine. The peaks at 7.91, 7.03, and 6.92 ppm are attributed to the ortho, meta, and para protons, respectively, of thiophenol molecules bound to the surface. A proton-detected <sup>13</sup>C spectrum of the thiophenol ligands on a CdS nanocrystal is shown in Figure 7b. In this spectrum, each multiplet of the proton spectrum is split into a doublet by the large, approximately 160 Hz, <sup>1</sup>H-<sup>13</sup>C *J* coupling. The artifacts between the doublets are due to incomplete suppression of the (99%) <sup>1</sup>H signal not coupled to a <sup>13</sup>C.

The solution-state proton NMR of other thiophenol cadmium sulfide compounds have been measured. We measured the <sup>1</sup>H NMR of the compounds Cd(SC<sub>6</sub>H<sub>5</sub>)<sub>2</sub> and (Cd(SC<sub>6</sub>H<sub>5</sub>)<sub>2</sub>)<sub>2</sub>-(H<sub>3</sub>CPCH<sub>2</sub>CH<sub>2</sub>PCH<sub>3</sub>)<sup>14</sup> and found that they show three peaks at almost exactly the same positions as those seen in our nanocrystals. Unfortunately, these compounds have nonmolecular crystal structures<sup>13,14</sup> which must rearrange when dissolved, which eliminates our ability to assign our spectra based on these models. Hagen, Stephan, and Holm<sup>15</sup> have presented <sup>1</sup>H NMR spectra of the molecule (Cd<sub>4</sub>(SC<sub>6</sub>H<sub>5</sub>)<sub>10</sub>)<sup>2-</sup>, which they deduce to have four terminal and six bridging thiophenols in solution. The <sup>1</sup>H NMR spectrum of this material measured at 322 K gave two lines at 6.85 and 7.31 ppm, which they assign to the ortho and meta/para peaks, respectively, of the thiophenol moieties. These resonances broaden as the temperature is lowered, indicating that exchange occurs between bridging and terminal positions. At the lowest temperature measured, 239 K, the thiophenol resonances are still coalesced and specific

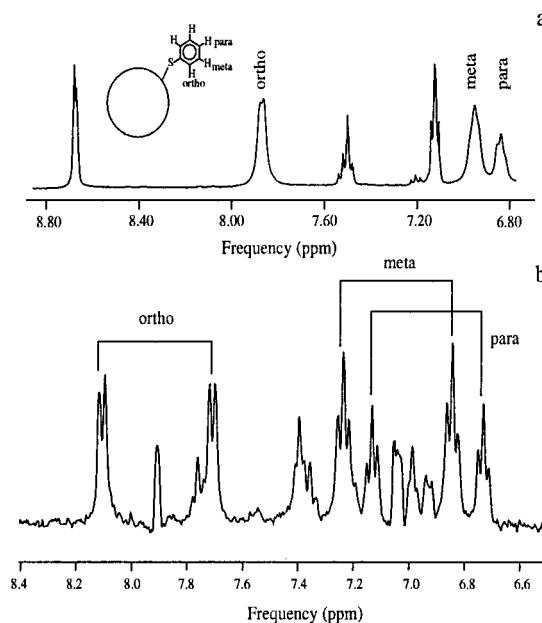


**Figure 7.** Representative NMR spectra. (a) <sup>1</sup>H spectra of thiophenol-capped CdS nanocrystals taken with 400.13 MHz spectrometer in 100% pyridine-*d*<sub>5</sub> at 303 K. (b) <sup>1</sup>H-detected <sup>13</sup>C spectrum of a 15.8 Å CdS nanocrystal taken with 400.13 MHz spectrometer in 100% pyridine-*d*<sub>5</sub> at 303 K. The double-INEPT sequence shown in Figure 5a was used. The sample was prepared by dissolving 5 mg of nanocrystal in 0.5 mL of pyridine-*d*<sub>5</sub> and then degassed. The sample had an approximate thiophenol concentration of 3.5 ± 0.5 mM. The recycle delay was 10 s. The <sup>1</sup>H 90° pulse length was 4.8 μs, the <sup>13</sup>C 90° pulse length was 10.0 μs, the first spin-lock length was 1 ms, and the second spin-lock length was 4 ms, which were adjusted empirically to obtain the best suppression of the residual proton signal. The delay  $\tau_J$  was 1.5625 ms. The spectrum was obtained in 512 scans and was apodized before Fourier transformation with a 2 Hz exponential filter. Each multiplet of the proton spectrum is now split by a carbon-proton *J*-coupling of approximately 160 Hz.

assignment of the chemical shifts for bridging and terminal sites could not be made.<sup>15</sup> The presence of exchange broadening indicates, however, that the bridging and terminally bound thiophenols give rise to distinguishable resonances, which might be observed in thiophenol-capped CdS nanocrystals. The observed resonances in the nanocrystals are significantly shifted from the resonances seen in the clusters produced by Hagen et al.,<sup>15</sup> indicating that we have predominately only one bonding geometry of thiophenol on the nanocrystal surface.

Changes in the <sup>1</sup>H spectrum over a period of days indicate that the surface of the nanocrystal slowly degrades. This was shown by the appearance of new peaks at 7.25, 7.38, and 8.34 ppm in the <sup>1</sup>H spectra and the disappearance of the peaks due to the bound thiophenol. The intensity of these new peaks is seen to increase with time, while the bound thiophenol peaks decrease with approximately the same rate. For particles in pyridine solution at room temperature, the bound thiophenol ligand resonances disappear completely in approximately 16 days. The same change in the NMR spectrum is seen in samples kept as powders but at a considerably slower rate. The degradation product has been identified as the dithiophenol, C<sub>5</sub>H<sub>5</sub>SSC<sub>5</sub>H<sub>5</sub>. Since this change requires both O<sub>2</sub> and UV light, if O<sub>2</sub> is excluded from the NMR tube, no reaction occurs and samples can be kept indefinitely.<sup>40</sup> Samples used in this study were usually sealed in tubes which had been degassed by repeating the freeze-pump-thaw procedure 5 times or were recorded without degassing within 1 week of particle synthesis. The figure and table captions indicate which preparation procedure was used for each sample. This degradation is very

**TABLE 2:  $^1\text{H}$  Longitudinal and Transverse Relaxation Times Measured for the Protons in the Thiophenol Ligands Attached to the Nanocrystal Surface<sup>a</sup>**

Longitudinal Relaxation Times				
particle radius $r$ (Å)	$T_1$ (s)			degassed <sup>b</sup>
	ortho	meta	para	
10.6	$5.8 \pm 0.3$	$6.2 \pm 0.3$	$6.6 \pm 0.3$	yes
15.2	$6.6 \pm 0.3$	$6.4 \pm 0.3$	$6.8 \pm 0.3$	yes
11.9	$3.7 \pm 0.2$	$2.9 \pm 0.2$	$2.9 \pm 0.2$	no
13.8	$3.4 \pm 0.2$	$3.1 \pm 0.2$	$2.9 \pm 0.2$	no
15.8	$4.1 \pm 0.2$	$3.4 \pm 0.2$	$3.2 \pm 0.2$	no
19.2	$5.0 \pm 0.2$	$3.3 \pm 0.2$	$3.7 \pm 0.2$	no

Transverse Relaxation Times for the Protons in the Thiophenol

Transverse Relaxation Times for the Protons in the Thiophenol				
particle radius $r$ (Å)	$T_2$ (ms)			degassed <sup>b</sup>
	ortho	meta	para	
10.6	$73 \pm 4$	$50 \pm 2$	$105 \pm 5$	yes
15.2	$127 \pm 6$	$80 \pm 4$	$240 \pm 12$	yes
11.9	$42 \pm 2$	$38 \pm 2$	$57 \pm 3$	no
13.8	$61 \pm 3$	$48 \pm 2$	$76 \pm 4$	no
15.8	$67 \pm 3$	$58 \pm 3$	$121 \pm 6$	no
19.2	$101 \pm 5$	$168 \pm 8^c$	$220 \pm 11$	no

<sup>a</sup> Measurement methods are described in the text. <sup>b</sup> If the samples were prepared in sealed tubes after having undergone 5 cycles of the freeze–pump–thaw procedure, they are referred to as degassed. Those samples which were exposed to atmospheric oxygen have a “no” in this column. <sup>c</sup> Significant degradation of this sample had occurred before this measurement could be performed. This was indicated by the appearance of the dithiophenol peaks in the spectrum.

**TABLE 3:  $^{13}\text{C}$  Longitudinal and Transverse Relaxation Times Measured for the Different Positions in the Thiophenol Ligands Attached to the Nanocrystal Surface<sup>a</sup>**

Longitudinal Relaxation Times			
$r$ (Å)	$T_1$ (s)		
	ortho	meta	para
10.6	$3.5 \pm 0.4$	$3.6 \pm 0.4$	$2.7 \pm 0.3$
15.2	$4.2 \pm 0.4$	$4.7 \pm 0.5$	$2.9 \pm 0.3$
Transverse Relaxation Times			
$r$ (Å)	$T_2$ (ms)		
	ortho	meta	para
10.6	$140 \pm 14$	$126 \pm 13$	$68 \pm 7$
15.2	$258 \pm 26$	$322 \pm 32$	$150 \pm 15$

<sup>a</sup> Measurement methods are described in the text. All samples were degassed.

similar to what has been reported by Majetich et al. in their studies of *n*-butanethiolate-capped CdSe nanocrystals.<sup>10</sup>

**Trends in the Relaxation Data and Thiophenol Bonding Configuration.** The measured values of  $T_2^{1\text{H}}$ , Table 2, range from 239 to 38 ms over all the studied samples and increase with nanocrystal radius. This is not the predicted behavior if the entire nanocrystal undergoes isotropic rotational diffusion as described by the Stokes–Einstein equation, with the thiophenol ligands fixed with respect to the nanocrystal surface. If this were the case, the transverse relaxation times would decrease with increasing nanocrystal radius. Moreover, if only nearest-neighbor intra-thiophenol dipole–dipole interactions are considered, this model also predicts that  $T_2^{1\text{H}_{\text{para}}} = T_2^{1\text{H}_{\text{meta}}} = 1/2 T_2^{1\text{H}_{\text{ortho}}}$  and that the carbon-13 transverse relaxation times would be equal as shown in Figure 2. None of these predictions are borne out in our data, Tables 2 and 3, indicating that the overall isotropic rotational diffusion of the nanocrystal does not dominate the thiophenol relaxation behavior and that internal

rotations of the Cd–S and S–C bonds must be included in the description in order to reproduce the experimental findings.

The degassed samples show that  $T_1^{1\text{H}}$  and  $T_1^{13\text{C}}$ , presented in Table 3, monotonically increase with nanocrystal radius, indicating that the nanocrystals are tumbling in the slow-motion regime. This is as expected for particles in a 400 MHz magnetic field whose overall tumbling time calculated using the Stokes–Einstein equation ranges from 1.7 to 7.1 ns, assuming that the viscosity of the solution is that of pure pyridine. The relative sizes of the longitudinal relaxation times provides us with some information about the bonding configuration and dynamics on the surface. The proton longitudinal relaxation times given in Table 2 show that all three rates are nearly equal and change order depending upon the nanocrystal radius, while the carbon relaxation times (Table 3) are always ordered ortho  $\approx$  meta  $>$  para. While the results of the theoretical calculations for both binding configurations presented in Figures 2–4 predict the observed ordering of the carbon longitudinal relaxation times as long as the internal correlation times are considerably shorter than the overall, the bridging model cannot predict the observed proton longitudinal relaxation times. The bridging model always predicts that the longitudinal relaxation time of the ortho proton is considerably longer than either the meta or para protons for physically reasonable internal correlation times. This is in direct contradiction to the measurement of almost equal longitudinal relaxation times in the protons.

The relative values of the transverse relaxation times, Tables 2 and 3 and Figures 2–4, can be understood in terms of partial averaging of the dipolar coupling caused by the rapid internal motion. For  $^{13}\text{C}$  relaxation in the bridging model, Table 3 and Figure 2, the C–H vector for the para carbon is not modulated by the rotation about the S–C bond. Thus, the dipolar coupling between these two nuclei is not averaged by this motion and overall tumbling of the nanocrystal causes a slow modulation of the full coupling, leading to rapid relaxation. For the ortho and meta carbons, the C–H dipolar coupling is partially averaged by the motion and the relaxation is, therefore, slower than for the para position. Similar arguments can also be applied to the  $^1\text{H}$  data, Table 2 and Figure 2, where the ortho–meta vector is not averaged by the rotation of the thiophenol while the meta to para vector is, leading to the prediction that the ortho proton relaxes faster than either the meta or para proton. In the case of a terminally bound thiophenol, the variation of the appropriate dipolar vector for the para  $^{13}\text{C}$  and the ortho  $^1\text{H}$  is modulated by rotation about the Cd–S bond; however, the magnitude of this fluctuation is much less than that for the other sites. While these arguments are only strictly valid in the fast-motion limit of the internal correlation time, partial averaging will even occur at longer internal correlation times.

**Fits of the Data to the Relaxation Models.** The predicted trends in the relaxation times are indeed observed in our data, presented in Tables 2 and 3. To provide a more quantitative estimate and to distinguish between models for bridging and terminal thiophenol ligands, fits to the degassed data were performed and the results of these fits are presented in Tables 4 and 5. The fits yield the correlation times for the overall tumbling of the nanocrystal and for the internal rotations. For neither motional model do the  $\chi^2$  values go below 1, indicating that the models do not perfectly predict our data; however, the fits to the terminal model give significantly lower values of  $\chi^2$  than the bridging model and the parameters are more physically reasonable.

In the fit of the bridging model, the overall correlation time,  $t_m$ , and the correlation time of the S–C bond,  $t_i$ , do not change

TABLE 4: Fits to Bridging Model<sup>a</sup>

fit parameters	nanocrystal radius			
	10.6 Å		15.2 Å	
$t_i$		$3.5 \times 10^{-12}$ s		$7.8 \times 10^{-12}$ s
$t_m$		$7.9 \times 10^{-9}$ s		$6.3 \times 10^{-9}$ s
$R_1^C$		$0.20$ s <sup>-1</sup>		$0.079$ s <sup>-1</sup>
$R_2^C$		$6.8$ s <sup>-1</sup>		$2.9$ s <sup>-1</sup>
$R_1^H$		$0.14$ s <sup>-1</sup>		$0.11$ s <sup>-1</sup>
$R_2^H$		$9.5$ s <sup>-1</sup>		$3.9$ s <sup>-1</sup>
$\chi^2$		10.8		15.2
best fit values	fit	experiment	fit	experiment
$T_1^C$ ortho	3.6 s	$3.5 \pm 0.4$ s	4.5 s	$4.2 \pm 0.4$ s
$T_1^C$ meta	3.6 s	$3.6 \pm 0.4$ s	4.5 s	$4.7 \pm 0.5$ s
$T_1^C$ para	0.395 s	$2.7 \pm 0.3$ s	0.338 s	$2.9 \pm 0.3$ s
$T_2^C$ ortho	135 ms	$140 \pm 14$ ms	286 ms	$258 \pm 26$ ms
$T_2^C$ meta	135 ms	$126 \pm 13$ ms	286 ms	$322 \pm 32$ ms
$T_2^C$ para	23 ms	$68 \pm 7$ ms	30 ms	$150 \pm 15$ ms
$T_1^H$ ortho	6.1 s	$5.8 \pm 0.3$ s	6.7 s	$6.6 \pm 0.3$ s
$T_1^H$ meta	5.8 s	$6.2 \pm 0.3$ s	6.1 s	$6.4 \pm 0.3$ s
$T_1^H$ para	6.6 s	$6.6 \pm 0.3$ s	6.9 s	$6.8 \pm 0.3$ s
$T_2^H$ ortho	56 ms	$73 \pm 4$ ms	95 ms	$127 \pm 6$ ms
$T_2^H$ meta	56 ms	$50 \pm 2$ ms	94 ms	$80 \pm 4$ ms
$T_2^H$ para	102 ms	$105 \pm 5$ ms	241 ms	$240 \pm 12$ ms

<sup>a</sup>  $R_1^C$ ,  $R_2^C$ ,  $R_1^H$ , and  $R_2^H$  are random-field relaxation rates included in the fits to account for relaxation mechanisms other than the explicitly included dipole–dipole mechanism.

TABLE 5: Fits to Terminal Model<sup>a</sup>

fit parameters	nanocrystal radius			
	10.6 Å		15.2 Å	
$t_{i1}$		$3.3 \times 10^{-11}$ s		$1.6 \times 10^{-11}$ s
$t_{i2}$		$1.4 \times 10^{-8}$ s		$1.3 \times 10^{-11}$ s
$t_m$		$1.7 \times 10^{-7}$ s		$1.1 \times 10^{-7}$ s
$R_1^C$		$0.0$ s <sup>-1</sup>		$0.16$ s <sup>-1</sup>
$R_2^C$		$0.0$ s <sup>-1</sup>		$3.0$ s <sup>-1</sup>
$R_1^H$		$0.11$ s <sup>-1</sup>		$0.13$ s <sup>-1</sup>
$R_2^H$		$6.5$ s <sup>-1</sup>		$4.0$ s <sup>-1</sup>
$\chi^2$		5.7		8.8
best-fit values	fit	experiment	fit	experiment
$T_1^C$ ortho	3.2 s	$3.5 \pm 0.4$ s	4.4 s	$4.2 \pm 0.4$ s
$T_1^C$ meta	3.2 s	$3.6 \pm 0.4$ s	4.4 s	$4.7 \pm 0.5$ s
$T_1^C$ para	3.0 s	$2.7 \pm 0.3$ s	3.0 s	$2.9 \pm 0.3$ s
$T_2^C$ ortho	125 ms	$140 \pm 14$ ms	286 ms	$258 \pm 26$ ms
$T_2^C$ meta	125 ms	$126 \pm 13$ ms	286 ms	$322 \pm 32$ ms
$T_2^C$ para	25 ms	$68 \pm 7$ ms	33 ms	$150 \pm 15$ ms
$T_1^H$ ortho	6.3 s	$5.8 \pm 0.3$ s	6.7 s	$6.6 \pm 0.3$ s
$T_1^H$ meta	5.6 s	$6.2 \pm 0.3$ s	6.2 s	$6.4 \pm 0.3$ s
$T_1^H$ para	6.6 s	$6.6 \pm 0.3$ s	6.9 s	$6.8 \pm 0.3$ s
$T_2^H$ ortho	63 ms	$73 \pm 4$ ms	97 ms	$127 \pm 6$ ms
$T_2^H$ meta	56 ms	$50 \pm 2$ ms	96 ms	$80 \pm 4$ ms
$T_2^H$ para	98 ms	$105 \pm 5$ ms	237 ms	$240 \pm 12$ ms

<sup>a</sup>  $R_1^C$ ,  $R_2^C$ ,  $R_1^H$ , and  $R_2^H$  are random-field relaxation rates included in the fits to account for relaxation mechanisms other than the explicitly included dipole–dipole mechanism.

significantly with nanocrystal radius while the random-field relaxation rates decrease significantly. For this model, it appears to be the random fields that force the model to fit and not the important parameters of the model. In the fit for terminally bound ligands, the overall correlation time,  $t_m$ , and the correlation time for rotation about the Cd–S bond,  $t_{i1}$ , remain constant while the correlation time of the S–C bond,  $t_{i2}$ , decreases by 3 orders of magnitude. The random-field relaxation rates slightly increase for the <sup>13</sup>C relaxation but remain roughly constant for the <sup>1</sup>H relaxation. For these reasons, we conclude that the data are most consistent with terminally bound thiophenol ligands.

The observation of decreasing internal correlation times with nanocrystal radius suggests that the energetic barriers to these

TABLE 6: Change in Relaxation Rates with Temperature<sup>a</sup>

peak	$T_2^{\text{high}}$ (ms)	$T_2^{\text{low}}$ (ms)	$T_2^{\text{high}}/T_2^{\text{low}}$
Transverse Relaxation Rates in 10.6 Å Thiophenol-Capped CdS Nanocrystals			
ortho	$63 \pm 3$	$73 \pm 4$	$0.86 \pm 0.06$
meta	$44 \pm 2$	$50 \pm 2$	$0.88 \pm 0.05$
para	$95 \pm 5$	$105 \pm 5$	$0.90 \pm 0.06$
Transverse Relaxation Rates in 15.2 Å Thiophenol-Capped CdS Nanocrystals			
ortho	$60 \pm 3$	$127 \pm 6$	$0.47 \pm 0.03$
meta	$44 \pm 2$	$80 \pm 4$	$0.55 \pm 0.04$
para	$83 \pm 4$	$240 \pm 12$	$0.35 \pm 0.02$

<sup>a</sup>  $T_2^{\text{low}}$  is the  $T_2$  measured at 25.9 °C, while  $T_2^{\text{high}}$  is that measured at 79.3 °C. Errors in  $T_2^{\text{high}}/T_2^{\text{low}}$  were calculated by propagating the errors in quadrature. All samples were degassed.

motions must be smaller in the larger nanocrystals. In previous studies,<sup>9</sup> we have shown that the coverage of the thiophenol ligands on the nanocrystal surface decreases as the nanocrystal radius increases, which is immediately consistent with the variation in the internal correlation times. As the coverage decreases, the steric hindrance between the thiophenols also decreases, allowing the ligands to rotate more freely. Our previous paper showed, however, that if the thiophenols were homogeneously distributed according to the measured coverages, the average distance between thiophenol ligands was much greater than the van der Waals radius of the thiophenol ligands. Thus, in order for the ligands to sterically hinder one another, they must be inhomogeneously distributed over the nanocrystal surface, leading to islands of thiophenol-covered regions which become progressively less dense with increasing radius.

**Influence of Additional Relaxation Mechanisms.** The random-field variables in our fits quantify the effects of all other relaxation mechanisms not included explicitly in our models, e.g., chemical-shift anisotropy, spin-rotation, and paramagnetic relaxation mechanisms. The values of the four random-field relaxation parameters in the fits where the thiophenol ligands are modeled as terminally bound contribute significantly to the transverse relaxation of the <sup>1</sup>H nuclei in both sizes studied and to <sup>13</sup>C transverse relaxation of the 15.2 Å radius nanocrystal. In all other cases they are consistently small. Since the random fields are assumed to be constant for the different sites in the molecule, the correct prediction of the relative values of the relaxation times indicates that the dipolar relaxation mechanism treated in this paper is indeed primarily responsible for the observed relaxation behavior.

Despite the success in modeling our data with the motions of a terminally bound thiophenol ligand, the temperature dependence of the <sup>1</sup>H transverse relaxation times is unusual and unexpected. The data, Table 6, show that  $T_2$  decreases as the temperature is increased and that the size of the effect increases in the larger nanocrystals. Since the motional model is successful at explaining the relative values of all the measured relaxation times, an additional mechanism must be proposed for the temperature dependence of the relaxation times that does not strongly depend on the molecular position of the nucleus under study. From the work of Hagen et al.<sup>15</sup> one might be tempted to explain the data by the onset of exchange between bridging and terminal bonding arrangements at the higher temperature. Such an explanation is not satisfactory because the bridging site is not seen in the spectrum at the higher temperature and the rate of exchange would not be expected to be such a strong function of nanocrystal radius. An alternative explanation for these data is that at higher temperatures electrons are being excited, leading to paramagnetic relaxation of the

thiophenol ligands. This excitation can occur either to the conduction band or surface-trap states. For the nuclei in a semiconductor, for example, the Si nuclei in a crystal of Si, it has been shown that the longitudinal relaxation time is affected by precisely this mechanism, where the coupling between the conduction band electron and the nuclei is provided by the Fermi contact interaction. Theory and experiment of the  $T_1$  of semiconductors have shown that the  $T_1 \propto T^{-1/2}$ , where  $T$  is the temperature of the sample.<sup>41</sup> A recent measurement of  $T_1$  and  $T_2$  in semiconductors by Vieth, Vega, Yellin, and Zamir has experimentally show that  $T_2$  in these systems is approximately proportional to  $T^{-2}$ .<sup>42</sup>

In the data presented in Table 4, the magnitude of the change in  $T_2^{1H}$  is greater for the larger particles than for the smaller ones. In our fits to the motional model for terminally bound thiophenol ligands, we also see the proton random fields are large and constant while the carbon random fields increase with nanocrystal radius. Both of these effects correlate with the measured decrease of the band gap with increasing nanocrystal radius, which implies that there should be more thermally excited electrons in the conduction bands of larger nanocrystals. For this reason, we propose that thermally excited conduction-band electrons make a significant contribution to the nuclear relaxation of the proton and carbon nuclei on the thiophenol ligands. Surface-trap states could also explain these results if the energy difference between the valence band and the trap scale with the nanocrystal size. More careful measurements and calculations need to be performed to verify this proposal.

## Conclusions

We have presented  $^1H$  and  $^{13}C$  NMR relaxation studies for the thiophenol ligands of CdS nanocrystals. The data provide a wealth of information on the surface structure and dynamics of these materials. First, the  $^1H$  and  $^{13}C$  NMR spectra demonstrate that there is predominately a single type of thiophenol on the nanocrystal surface. While the simple 1D spectra are not easily assigned to the possible bonding arrangements of the thiophenol ligands, an analysis of the relaxation data as a function of nanocrystal radius suggest that the thiophenol ligands are terminally bound. From the variation of the internal correlation times with nanocrystal radius, the rotation of the thiophenol about the Cd-S bond is seen to be increasingly hindered as the nanocrystal radius decreases. This implies that the distribution of thiophenol ligands on the surface is not homogeneous, but rather the thiophenol ligands form islands on the surface. The motion could be further sterically hindered by the solvent pyridine, which is thought to be rapidly exchanging on and off the surface. These islands of covered nanocrystal surface could profoundly influence the properties of the nanocrystal. Uncovered regions of the nanocrystal could provide trap sites on the surface,<sup>8</sup> and influence a permanent dipole moment of the ground state.

The anomalous temperature dependence of transverse relaxation is governed by an additional mechanism. A possible mechanism is paramagnetic relaxation of the  $^1H$  by a thermally populated paramagnetic state of the nanocrystal. Since the relaxation rate predicted by this mechanism depends on the electronic population thermally excited into the conduction band, it should scale directly with the band gap of the nanocrystal. Consistent with this theory, the data demonstrate that the smaller nanocrystals have smaller changes in the relaxation rates than do the larger particles. This behavior should be a general property of all semiconductor nanocrystals and suggests that the relaxation behavior of the nanocrystal ligands can act as a

probe of the nanocrystal electronic state. For example, the relaxation behavior appears to be sensitive to the radius and the number of charge carriers in the nanocrystal.

Previously, detailed information about the structure and dynamics of surface capping molecules on nanocrystal surfaces has been difficult to obtain. NMR appears to be an ideal tool for extracting this information, which is needed in order to fully understand such properties of the nanocrystal as ultrafast trapping of photon-generated electrons and holes.<sup>43-46</sup> By binding organic molecules to the surface, one hopes to move all mid- or near-band-gap surface states to much higher energies and quench this surface trapping. Clearly, to accomplish this, the coverage will need to be increased to saturation and the effects of these changes on the surface can be monitored by NMR.

**Acknowledgment.** J.R.S. is grateful to Zoran Kurtovic for helpful discussions and to Alexander Pines for continuing advice and support. This research was funded by the Director, Office of Energy Research, Office of Basic Energy Sciences, Materials Sciences Division of the U.S. Department of Energy, under Contract No. DE-AC03-76SF00098.

## Appendix 1

To find the conditional probability for rotational diffusion of the thiophenol ligand about its sulfur-carbon bond, the diffusion equation

$$\frac{\partial p(\gamma', t | \gamma, 0)}{\partial t} = \left(\frac{1}{t_i}\right) \frac{\partial^2 p(\gamma', t | \gamma, 0)}{\partial \gamma'^2} \quad (\text{A1-1})$$

must be solved, where  $t_i$  is the correlation time for the internal motion. We assume a delta function initial condition

$$p(\gamma', 0 | \gamma, 0) = \delta(\gamma' - \gamma) \quad (\text{A1-2})$$

and periodic boundary conditions

$$p(0, t | 0, 0) = p(2\pi, t | 0, 0) \quad (\text{A1-3})$$

The periodic boundary conditions imply a Fourier series expansion of the conditional probability

$$p(\gamma', t | \gamma, 0) = \frac{1}{2} a_0(t) + \sum_{m=1}^{\infty} \{a_m(t) \cos[m(\gamma' - \gamma)] + b_m(t) \sin[m(\gamma' - \gamma)]\} \quad (\text{A1-4})$$

where the Fourier coefficients are given by

$$a_n(t) = \frac{1}{\pi} \int_{-\pi}^{\pi} p(\gamma', t | \gamma, 0) \cos[n(\gamma' - \gamma)] d\gamma' \quad n \geq 0 \quad (\text{A1-5})$$

and

$$b_n(t) = \frac{1}{\pi} \int_{-\pi}^{\pi} p(\gamma', t | \gamma, 0) \sin[n(\gamma' - \gamma)] d\gamma' \quad n > 0 \quad (\text{A1-6})$$

By substituting the Fourier expansion of the conditional probability into the diffusion equation, an infinite number of differential equations, one for each  $a_m(t)$  and  $b_m(t)$ , is produced

$$\frac{1}{2} \frac{\partial a_0(t)}{\partial t} + \sum_{m=1}^{\infty} \left\{ \frac{\partial a_m(t)}{\partial t} \cos[m(\gamma' - \gamma)] + \frac{\partial b_m(t)}{\partial t} \sin[m(\gamma' - \gamma)] \right\} = - \left( \frac{1}{t_i} \right) \sum_{m=1}^{\infty} m^2 \{ a_m(t) \cos[m(\gamma' - \gamma)] + b_m(t) \sin[m(\gamma' - \gamma)] \} \quad (\text{A1-7})$$

The differential equation for  $m = 0$  is  $(\partial a_0(t))/(\partial t) = 0$ , which implies that  $a_0(t) = \text{constant}$ . When  $m \neq 0$ , we find the differential equations

$$\frac{\partial a_m(t)}{\partial t} = - \left( \frac{1}{t_i} \right) m^2 a_m(t) \quad (\text{A1-8})$$

and

$$\frac{\partial b_m(t)}{\partial t} = - \left( \frac{1}{t_i} \right) m^2 b_m(t) \quad (\text{A1-9})$$

Integrating these equations gives

$$a_m(t) = a_m(0) e^{-m^2 t/t_i} \quad (\text{A1-10})$$

and

$$b_m(t) = b_m(0) e^{-m^2 t/t_i} \quad (\text{A1-11})$$

The preexponential factors  $a_m(0)$  and  $b_m(0)$  are given by

$$a_m(0) = \frac{1}{\pi} \int_{-\pi}^{\pi} \delta(\gamma' - \gamma) \cos[m(\gamma' - \gamma)] d\gamma' = \frac{1}{\pi} \quad (\text{A1-12})$$

and

$$b_m(0) = \frac{1}{\pi} \int_{-\pi}^{\pi} \delta(\gamma' - \gamma) \sin[m(\gamma' - \gamma)] d\gamma' = 0 \quad (\text{A1-13})$$

for all  $m$ . Thus, we find that the conditional probability for rotational diffusion is

$$p(\gamma', t | \gamma, 0) = \frac{1}{2\pi} + \frac{1}{\pi} \sum_{m=1}^{\infty} e^{-m^2 t/t_i} \cos[m(\gamma' - \gamma)] \quad (\text{A1-14})$$

which simplifies in the long-time limit to

$$p(\gamma', t | \gamma, 0) = \frac{1}{2\pi} + \frac{1}{\pi} e^{-t/t_i} \cos(\gamma' - \gamma) \quad (\text{A1-15})$$

## Appendix 2

In the calculation of the spectral density function for a terminal thiophenol, there are two degrees of freedom. Expanding the spherical harmonics describing the orientation of the internuclear vector in the laboratory frame into the particle and molecular frames defined in Figure 1b gives

$$Y_{2,q}(\theta_{LF}^{ij}(t), \phi_{LF}^{ij}(t)) = \sum_{m,n,l} D_{q,m}^{(2)}(\Omega_{L \rightarrow P}(t)) D_{m,n}^{(2)}(\Omega_{P \rightarrow M1}(t)) \times D_{n,l}^{(2)}(\Omega_{M1 \rightarrow M2}(t)) Y_{2,l}(\theta_{M2 \rightarrow PAS}^{ij}, \phi_{M2 \rightarrow PAS}^{ij}) \quad (\text{A2-1})$$

Since motion about both the Cd-S and the S-C bonds is now possible, this transformation requires one more rotation than in the bridging case. The new frames  $M1$  and  $M2$  refer to an axis system where the  $z$ -axis is along the Cd-S and S-C bonds, respectively. In the case of the  $M2$  axis system, the  $x$ -axis is assumed to be in the plane defined by the phenol ring of the thiophenol. The  $\gamma$  euler angles of  $\Omega_{P \rightarrow M1} = \{\alpha_{P \rightarrow M1}, \beta_{P \rightarrow M1}, \gamma_{P \rightarrow M1}\}$  and  $\Omega_{M1 \rightarrow M2} = \{\alpha_{M1 \rightarrow M2}, \beta_{M1 \rightarrow M2}, \gamma_{M1 \rightarrow M2}\}$  are time dependent and reflect the motion about the Cd-S and S-C bonds, respectively. This expansion of the spherical harmonics is put into the expression for the correlation function, eq 2. If the overall tumbling of the nanocrystal and both of the two internal rotations are all assumed to be uncorrelated from one another, we obtain

$$C_q(t) = \frac{\pi}{5} \omega_D^2 \sum_{\substack{m',n',l' \\ m,n,l}} \langle D_{q,m}^{(2)}(\Omega_{L \rightarrow P}) D_{q,m'}^{(2)}(\Omega'_{L \rightarrow P})^* \rangle \times \langle D_{m,n}^{(2)}(\Omega_{P \rightarrow M1}) D_{m',n'}^{(2)}(\Omega'_{P \rightarrow M1})^* \rangle \langle D_{n,l}^{(2)}(\Omega_{M1 \rightarrow M2}) \times D_{n',l'}^{(2)}(\Omega'_{M1 \rightarrow M2})^* \rangle Y_{2,l}(\theta_{M2 \rightarrow PAS}^{ij}, 0) Y_{2,l'}(\theta_{M2 \rightarrow PAS}^{ij}, 0)^* \quad (\text{A2-2})$$

Again using eqs 5, 6, and 7, equation A2-2 becomes

$$C(t) = \frac{\pi}{25} \omega_D^2 e^{-t/\tau_m} \sum_{n,l,l'} d_{n,l}^{(2)}(\beta_{M1 \rightarrow M2}) d_{n,l'}^{(2)}(\beta_{M1 \rightarrow M2}) \times \langle e^{in(\gamma'_1 - \gamma_1)} \rangle \langle e^{i(l'\gamma'_2 - l\gamma_2)} \rangle Y_{2,l}(\theta_{M2 \rightarrow PAS}^{ij}, 0) Y_{2,l'}(\theta_{M2 \rightarrow PAS}^{ij}, 0)^* \quad (\text{A2-3})$$

As in the bridging case, isotropic tumbling of the nanocrystal makes the index  $q$  irrelevant. The real part of this equation simplifies to

$$C(t) = \frac{\pi}{25} \omega_D^2 e^{-t/\tau_m} \sum_{n,l,l'} d_{n,l}^{(2)}(\beta_{M1 \rightarrow M2}) d_{n,l'}^{(2)}(\beta_{M1 \rightarrow M2}) \times |Y_{2,l}(\theta_{M2 \rightarrow PAS}^{ij}, 0)|^2 \{ \langle \cos\{n(\gamma'_1 - \gamma_1)\} \rangle \langle \cos\{l'\gamma'_2 - l\gamma_2\} \rangle - \langle \sin\{n(\gamma'_1 - \gamma_1)\} \rangle \langle \sin\{l'\gamma'_2 - l\gamma_2\} \rangle \} \quad (\text{A2-4})$$

The ensemble average  $\langle \sin\{n(\gamma'_1 - \gamma_1)\} \rangle$  is zero since the integrand is odd. This implies that only the two cosine integrals need to be explicitly evaluated. The integral  $\langle \cos\{n(\gamma'_1 - \gamma_1)\} \rangle$  is given by eq 12, with the replacement of  $t_i$  with  $t_{i1}$ . The integral  $\langle \cos\{l'\gamma'_2 - l\gamma_2\} \rangle$  is found to be

$$\langle \cos\{l'\gamma'_2 - l\gamma_2\} \rangle = \frac{1}{2\pi^2} \int_0^{2\pi} \int_0^{2\pi} \left[ \frac{1}{2} + e^{-t/t_{i2}} \cos\{\gamma'_2 - \gamma_2\} \right] \cos\{l'\gamma'_2 - l\gamma_2\} d\gamma'_2 d\gamma_2 = \begin{cases} 1 & \text{for } l = l' = 0 \\ e^{-t/t_{i2}} & \text{for } l = l' = \pm 1 \\ 0 & \text{for all other cases} \end{cases} \quad (\text{A2-5})$$

By inserting eqs 12 and A2-5 into equation A2-4, the correlation function for a terminal thiophenol is found to be

$$\begin{aligned}
C(t) = & \frac{\pi}{25} \omega_D^2 \{ |d_{0,0}^{(2)}(\beta_{M1 \rightarrow M2})|^2 |Y_{2,0}(\theta_{M2 \rightarrow PAS}^{ij}, 0)|^2 e^{-t/t_m} + \\
& 2 |d_{1,0}^{(2)}(\beta_{M1 \rightarrow M2})|^2 |Y_{2,0}(\theta_{M2 \rightarrow PAS}^{ij}, 0)|^2 e^{-t(1/t_m + 1/t_{i1})} + \\
& 2 |d_{1,0}^{(2)}(\beta_{M1 \rightarrow M2})|^2 |Y_{2,1}(\theta_{M2 \rightarrow PAS}^{ij}, 0)|^2 e^{-t(1/t_m + 1/t_{i2})} + \\
& 2(|d_{1,1}^{(2)}(\beta_{M1 \rightarrow M2})|^2 + |d_{1,-1}^{(2)}(\beta_{M1 \rightarrow M2})|^2) \times \\
& |Y_{2,1}(\theta_{M2 \rightarrow PAS}^{ij}, 0)|^2 e^{-t(1/t_m + 1/t_{i1} + 1/t_{i2})} \} \quad (\text{A2-6})
\end{aligned}$$

## References and Notes

- (1) Shiang, J. J.; Goldstein, A. N.; Alivisatos, A. P. *J. Chem. Phys.* **1990**, *92*, 3232.
- (2) Colvin, V. L.; Alivisatos, A. P.; Tobin, J. G. *Phys. Rev. Lett.* **1991**, *66*, 2786.
- (3) Shimitt-Rink, S.; Miller, D. A. B.; Chemla, D. S. *Phys. Rev. B* **1987**, *35*, 8113.
- (4) Miller, D. A. B.; Chemla, D. S.; Shimitt-Rink, S. *Phys. Rev. B* **1986**, *33*, 6976.
- (5) Colvin, V. L.; Schlamp, M. C.; Alivisatos, A. P. *Nature* **1994**, *370*, 354.
- (6) Tolbert, S. H.; Alivisatos, A. P. *Science* **1994**, *265*, 373.
- (7) Katari, J. E. B.; Colvin, V. L.; Alivisatos, A. P. *J. Phys. Chem.* **1994**, *98*, 4109.
- (8) Becerra, L. R.; Murray, C. B.; Griffin, R. G.; Bawendi, M. G. *J. Chem. Phys.* **1994**, *100*, 3297.
- (9) Sachleben, J. R.; Wooten, E. W.; Emsley, L.; Pines, A.; Colvin, V.; Alivisatos, A. P. *Chem. Phys. Lett.* **1992**, *198*, 431.
- (10) Majetich, S. A.; Carter, A. C.; Belot, J.; McCullough, R. D. *J. Phys. Chem.* **1994**, *98*, 13705.
- (11) Woessner, D. E. *J. Chem. Phys.* **1962**, *36*, 1.
- (12) Woessner, D. E. *J. Chem. Phys.* **1962**, *37*, 647.
- (13) Dance, I. G.; Choy, A.; Scudder, M. L. *J. Am. Chem. Soc.* **1984**, *106*, 6285.
- (14) Craig, D.; Dance, I.; Garbutt, R. *Angew. Chem., Int. Ed. Engl.* **1986**, *25*, 165.
- (15) Hagen, K. S.; Stephan, D. W.; Holm, R. H. *Inorg. Chem.* **1982**, *21*, 3928.
- (16) Herron, N.; Calabrese, J. C.; Farneth, W. E.; Wang, Y. *Science* **1993**, *259*, 1426.
- (17) Redfield, A. G. In *Advances in Magnetic Resonance*; Waugh, J., Ed.; Vol. 1, p 1.
- (18) Redfield, A. G. *Phys. Rev.* **1955**, *98*, 1787.
- (19) Redfield, A. G. *IBM J. Res. Dev.* **1957**, *1*, 19.
- (20) Wittebort, R. J.; Szabo, A. *J. Chem. Phys.* **1978**, *69*, 1722.
- (21) Varshalovich, D. A.; Moskalev, A. N.; Khersonskii, V. K. *Quantum Theory of Angular Momentum*; World Scientific: Singapore, 1988.
- (22) Rose, M. E. *Elementary Theory of Angular Momentum*; Wiley: New York, 1955.
- (23) Edmonds, A. R. *Angular Momentum in Quantum Mechanics* 2nd ed.; Princeton University Press: Princeton, NJ, 1974; Vol. 4.
- (24) Colvin, V. L.; Goldstein, A. N.; Alivisatos, A. P. *J. Am. Chem. Soc.* **1992**, *114*, 5221.
- (25) Lianos, P.; Thomas, J. K. *Chem. Phys. Lett.* **1986**, *125*, 299.
- (26) Steigerwald, M. L.; Alivisatos, A. P.; Gibson, J. M.; Harris, T. D.; Kortan, R.; Muller, A. J.; Thayer, A. M.; Duncan, T. M.; Douglass, D. C.; Brus, L. E. *J. Am. Chem. Soc.* **1988**, *110*, 3046.
- (27) Emsley, L.; Kowalewski, J.; Bodenhausen, G. *Appl. Magn. Res.* **1990**, *1*, 139.
- (28) Emsley, L.; Bodenhausen, G. *J. Magn. Reson.* **1989**, *82*, 211.
- (29) Emsley, L.; Bodenhausen, G. *Chem. Phys. Lett.* **1990**, *165*, 469.
- (30) Ernst, R.; Bodenhausen, G.; Wokaun, A. *Principles of Nuclear Magnetic Resonance in One and Two Dimensions*; Clarendon Press: Oxford, 1987.
- (31) Vidusek, D. A.; Roberts, M. F.; Bodenhausen, G. *J. Am. Chem. Soc.* **1982**, *104*, 5452.
- (32) Roberts, M. F.; Vidusek, D. A.; Bodenhausen, G. *FEBS Lett.* **1980**, *117*, 311.
- (33) Redfield, A. J. *Chem. Phys. Lett.* **1983**, *96*, 537.
- (34) Morris, G. A.; Freeman, R. *J. Am. Chem. Soc.* **1979**, *101*, 760.
- (35) Burum, D. P.; Ernst, R. R. *J. Magn. Reson.* **1980**, *39*, 163.
- (36) Bodenhausen, G.; Ruben, D. *J. Chem. Phys. Lett.* **1980**, *69*, 185.
- (37) Doddrell, D.; Glushko, V.; Allerhand, A. *J. Chem. Phys.* **1972**, *56*, 3683.
- (38) *CRC Handbook of Chemistry and Physics*, 66th ed.; CRC Press: Boca Raton, FL, 1985.
- (39) Press, W. H.; Teukolsky, S. A.; Vetterling, W. T.; Flannery, B. P. *Numerical Recipes in C: The Art of Scientific Computing*, 2nd ed.; Cambridge University Press: Cambridge, 1992.
- (40) Bowers, C. R.; Grubbs, R.; Sachleben, J. R.; Alivisatos, A. P. Unpublished data.
- (41) Abragam, A. *Principles of Nuclear Magnetism*; Clarendon Press: Oxford, 1989; Vol. 32.
- (42) Vieth, H. M.; Vega, S.; Yellin, N.; Zamir, D. *J. Phys. Chem.* **1991**, *95*, 1420.
- (43) Alivisatos, A. P.; Harris, A.; Levinos, N.; Steigerwald, M. L.; Brus, L. E. *J. Chem. Phys.* **1989**, *89*, 4001.
- (44) Bawendi, M. G.; Wilson, W. L.; Rothberg, L.; Carrol, P. J.; Jedju, T. M.; Steigerwald, M. L.; Brus, L. E. *Phys. Rev. Lett.* **1990**, *65*, 1623.
- (45) Bawendi, M. G.; Carrol, P. J.; Wilson, W. L.; Brus, L. E. *J. Chem. Phys.* **1992**, *96*, 946.
- (46) Peyghambarian, P.; Fluefel, B.; Hulin, D.; Migus, A.; Joffe, M.; Antonetti, A.; Koch, S. W.; Lindberg, M. *J. Quantum Electron.* **1989**, *25*, 2516.